ZnO nanorods prepared via ablation of Zn with millisecond laser in liquid media

Mitsuhiro Honda[a,d], Taku Goto[c], Tatsuki Owashi[b], Alex G. Rozhin[e],
Shigeru Yamaguchi[a], Tsuyohito Ito[c], Sergei A. Kulinich[a,e,*]

[a] *Institute of Innovative Science and Technology, Tokai University, Hiratsuka, Kanagawa, 259-1292, Japan*

[b] *Department of Mechanical Engineering, Tokai University, Hiratsuka, Kanagawa, 259-1292, Japan*

[c] *Graduate School of Engineering, Osaka University, Suita, Osaka, 565-0871, Japan*

[d] *Graduate School of Engineering, Nagoya Institute of Technology, Nagoya, Aichi, 466-8555, Japan*

[e] *Nanoscience Research Group, Aston Institute of Photonic Technologies, School of Engineering and Applied Science, Aston University, Birmingham, B4 7ET, UK*

Abstract

ZnO nanomaterials with controlled size, shape and surface chemistry are required for applications in diverse areas, such as optoelectronics, photocatalysis, biomedicine and so on. Here, we report on ZnO nanostructures with rod-like and spherical shapes prepared via laser ablation in liquid using a laser with millisecond-long pulses. By changing laser parameters (such as pulse width and peak power), the size or aspect ratio of such nanostructures could be tuned. The surface chemistry and defects of the products were also strongly affected by applied laser conditions. The preparation of different structures is explained by the effect of intense heat and/or pressure of liquid media caused by millisecond-long pulses.

* Corresponding author. Email: skulinich@tokai-u.jp (S.A. Kulinich).

1. Introduction

In the last decade, laser ablation in liquid (LAL) has proven to be an attractive, simple, and efficient technique to generate a large variety of nanostructures of diverse materials [1-16]. In this approach, laser beam is typically focused on a solid (often metal) target immersed into a liquid and produces various nanostructures whose chemistry, morphology and size distribution are defined by both the laser pulse parameters and the liquid [1,2,17]. This technique is attractive as a green approach using minimum solvents, easy-to-use, and even sometimes capable of controlling the morphology of produced nanomaterials [1,2,6,8,14]. The recent use of high pressures, i.e. ablating in pressurized cells, permits to expand the technique and allows for more control over the product [17-20].

ZnO is one of the most versatile materials with various potential applications in nanotechnology and other related fields, as this environmentally friendly semiconductor has a great potential in optics and optoelectronics, photocatalysis, energy conversion, biomedicine, and so on [3,6,7,9,10,18,21-31]. Amongst metal oxides, ZnO is probably one of the most investigated semiconductor materials and accordingly its nanostructures have been synthesized by various methods, such as (to name a few) solvothermal synthesis [22-24,27,30-32], microwave irradiation [31,33], and CVD [26,27]. The LAL method was also applied, and both doped and non-doped, as well as surface-stabilized or non-stabilized, ZnO nanoparticles (NPs) with different morphologies and sizes were reported [4-10,12,14-18,34-36].

In most cases, nanosecond pulsed lasers were applied [4-7,9,12], with little work done exploiting either femtosecond or picosecond [34,36] or millisecond lasers [3,8,14] with shorter and longer pulses, respectively. This work deals with the preparation of ZnO nanostructures by means of millisecond pulsed laser. Since the pulse produced by millisecond lasers is much longer compared to heat propagation in solids, the temperature of ablated target is expected to rise, generating intense heating of surrounding

liquid, and consequently influencing the produced nanostructures. As liquid media, water and ethanol were used. Varying laser beam parameters, the effect of liquid media and beam parameters on the produced nanostructures was studied. The product was characterized by means of several microscopic and spectroscopic techniques. It is shown that ZnO nanorods or nanospheres can be prepared in one step when water or ethanol are used as media, which was not observed when laser beams with shorter pulses were applied [5,6,17,18,34].

2. Experimental procedures

The experimental setup used in this work is schematically illustrated in Fig.1. Zinc plates (99.5 % purity, 2 mm thick) were placed vertically into a quartz cuvette and used as a target. The size of the cuvette was 30 mm x 30 mm x 50 mm, with the wall thickness of 2 mm. The amount of liquid used was typically ~15 ml. A millisecond pulsed Nd:YAG laser with the wavelength of 1064 nm was applied to irradiate the target through the cuvette side wall, its beam being focused on the Zn plate surface by means of a lens with the focal length of 9.0 cm. The focused beam diameter was 150 μm. The applied pulse peak power was 1 and 5 kW, while the pulse width was changed from 0.5 to 2 ms. All the samples were prepared for 30 min, while no medium agitation was applied.

The prepared nanostructures were drop-cast on Cu grids for further observations with transmission electron microscopy (TEM, HF-2200 from Hitachi). Upon centrifugation (16,500 rpm, 15 min), the prepared suspensions were cast on a Si substrate and then characterized by means of X-ray photoelectron spectroscopy (XPS, Quantum 2000, ULVAC-PHI), X-ray diffractometry (XRD, D8 Discover from Bruker) and photoluminescence (PL) spectroscopy. For PL measurements, a homemade system previously described elsewhere was used [17,18]. The PL measurements were conducted at room

temperature with a He-Cd laser (325 nm) as excitation source and using dry ZnO NPs drop-cast on Si wafers. Absorption spectra of the obtained suspensions were recorded in a UV-vis spectrometer (UV-2450 from Shimadzu).

3. Results and discussion

Figures 2a-f present TEM images of ZnO nanomaterials prepared upon ablating Zn targets in water for 30 min with different values of pulse width (0.5, 1 and 2 ms) and peak energy (1 and 5 kW). It is well seen in Figs.2a-f that under the applied conditions the products prepared in water tended to be rod-shaped. As the pulse width and peak power were varied, both size and shape of the nanostructures were observed to change. In order to investigate the effect of laser parameters on the size and aspect ratio of ZnO nanorods, the TEM images of the samples were used to measure their geometrical parameters.

The influence of pulse width on the size and aspect ratio of prepared nanorods is shown in Figs.2g,h, where red and blue symbols stand for peak powers of 1 and 5 kW, respectively. In Fig.2g, open circles and triangles indicate the length and the width of ZnO nanorods prepared in water, with the aspect ratio being shown in Fig.2h. The size of ZnO nanorods is seen in Fig.2g to change with both the pulse width and peak power used. The nanorod length is seen to increase and saturate with the increase in pulse width from 0.5 to 2 ms (see red and blue circles in Fig.2g), while the nanorod width changes less and mainly remains between 30 and 50 nm (red and blue triangles in Fig.2g). At pulse peak power of 5 kW, the size of prepared nanorods is seen to increase in both dimensions as the pulse width changes from 0.5 to 1 ms, while no noticeable changes in size are observed when longer pulses (2 ms) are applied. In Fig.2h it is seen that ZnO nanorods with a wide range of aspect ratios, from 1.6 to 6, were prepared in our experiments. When pulse width was raised from 0.5 to 1 ms, the aspect ratio is seen in Fig.2h to rise. At

lower peak power of 1 kW (red symbols in Fig.2h), the aspect ratio was then observed to drop at a pulse width value of 2 ms. At the same time, at a higher peak power of 5 kW, no such a drop in aspect ratio was observed between pulse width values of 1 and 2 ms. It is thus seen that the use of millisecond-long pulses allows for a wide control over the aspect ratio of ZnO nanorods, which was never reported in the previous studies where mainly nanosecond and femptosecond pulsed lasers were utilized.

The products prepared in pure ethanol were also studied by TEM. Figures 3a-c and Fig.3d show TEM images of such samples and how their size was influenced by pulse width, respectively. When ethanol was used as a liquid medium, only spherically-shaped NPs were found in the product, as well seen in Figs.3a-c. Similar to their counterparts prepared in water, the size of NPs prepared in ethanol was also governed by pulse width (see Fig.3d). With increase in pulse width from 0.5 to 2 ms, the NP diameter tended to increase.

The above-mentioned changes in product shapes and sizes observed in Fig.2 and Fig.3 are believed to be resulted from different liquid medium parameters and medium chemistry during the evaporation, oxidation and agglomeration of ablated Zn species, as all such stages occur following the laser beam hit on Zn target in either water or ethanol. The shape, size and chemistry of products prepared via LAL are known to be a complex function of numerous variables, such as: the nature of liquid environment, laser pulse parameters, changes in growth temperature and temperature gradients, surface energy of forming species, availability of surfactant molecules and so on [1,2,7,8,17]. Longer laser pulses are known to heat metal targets intensively [8,14], which agrees well with our observations. We speculate that the ZnO rods prepared in water media, as well as their growth along the longitudinal axis, are directly related to elevated temperatures observed during our experiments and caused by the use of longer laser pulses. As an example, when the pulse width was changed from 0.5 to 1 ms, the medium temperature was

found to increase from 40 to 80 °C, and from 80 to 90 °C at pulse peak power of 1 and 5 kW, respectively.

The formation of ZnO nanorods and their elongation at elevated temperatures was previously reported by Ishikawa and coworkers, who ablated ZnO in neat water with a nano-second pulsed laser in a setup heated to 60-80 °C by an external source [7]. Their findings generally agree with our observations, implying that the elevated medium temperatures were among the reasons for both the formation of rod-shaped ZnO NPs and the increase of their aspect ratio observed in Fig.2g. The main difference between our experiments and those of Ishikawa and coauthors was the absence of any external heating in our case as millisecond-long pulses provided a heating effect by themselves. As shown in Supplementary Information Fig.S1 and Fig.2a,b, when water medium was cooled down (by using ice) during ablation, spherically-shaped ZnO NPs were prepared instead of nanorods, which fully supports the above assumption. This also agrees well with the conclusions of Ishikawa *at al.* who proposed that small spherical NPs of ZnO are formed during laser ablation of Zn in pure water at room temperature, while at elevated temperatures such small nanocrystals recrystallize into larger rod-like nanostructures [7]. Thus, the temperature of water medium is very crucial for nanorod growth. The advantage of our approach is that no external heating was needed to keep medium temperatures around 60-80 °C, as this temperature range was naturally achieved via ablating the target with longer pulses.

In general, there are at least two parameters to be considered as playing crucial role in NP formation in our experiments, those being medium temperature and secondary irradiation of already formed structures. The temperature rise caused by longer pulses and higher pulse peak power was already mentioned above. As a high-surface-energy material, small ZnO NPs are well known to tend to agglomerate in the absence of any surface modifiers or surfactant that would stabilize their surface and suppress further agglomeration [7,18]. This process is accelerated by elevated temperatures which

stimulate the growth along the fastest-growing direction of the hexagonal wurtzite ZnO phase, i.e. the [0001] direction [26,28,37-40]. When the applied laser conditions allowed for a certain temperature raise, caused by target heating, nanostructures with similar sizes and shapes were observed (see Fig.2.g, the data for products prepared at 1kW and 2 ms, 5kW and pulse widths longer than 1 ms). Note that in all such cases, the measured temperatures during ablation were quite similar, typically reaching ~70-80 ^{o}C.

The second parameter is secondary irradiation of produced nanostructures [1,2,8], which occurs when the already formed structures are subjected to irradiation by subsequent laser pulses. The probability of such irradiation should be higher at longer pulse duration, while its effect is expected to be stronger at higher pulse peak energy. In Fig.2g, this effect is believed to be seen as all the nanorods produced at 5 kW (blue circles) and longer pulse duration values of 1 and 2 ms are shorter than those prepared at 1 kW (red circles). In addition, it should be noted that when the secondary irradiation fragments NPs and makes them smaller, the size distribution of the product should be somewhat wider, which indeed is observed in Fig.2g for the products prepared at 5 kW and with pulse duration of 1 and 2 ms.

The trends presented in Fig.2h are believed to represent all the complexity of various factors affecting the formation of nanomaterials during LAL processes, in particular the impact of the two above mentioned factors. On one hand, longer pulses should lead to a stronger heating effect through energy absorption by the Zn target, which in turn should result in longer and larger ZnO nanorods. On the other hand, longer pulses should increase the risk of secondary irradiation (and thus partial fragmentation) of already-formed nanostructures, thus making them smaller. One can assume that between 0.5 and 1 ms, the former effect dominates, while between 1 and 2 ms, the latter (partial defragmentation caused by secondary irradiation) manifests itself (see Figs.2g,h). The assumption on the effect of secondary irradiation is also supported by the fact that the ZnO nanorods produced at 5 kW were never as long as

those produced at 1 kW (see Figs.2g,h). The nanorods with the highest aspect ratio (of ~6) obtained at 1 kW and 1 ms (as peak power and pulse width, respectively) are believed to be a result of the two above trends: elevated medium temperatures at pulse widths above 1 ms and stronger secondary irradiation (and fragmentation of already-formed nanostructures) at longer pulse durations and higher power.

The fact that the NPs presented in Fig.3 and prepared in pure ethanol were spherical and somewhat smaller than those presented in Fig.2 (prepared in water) implies that the mechanisms involved into formation of such NPs are somewhat different. On one hand, the oxidizing potential of ethanol, when compared to that of water, is well known to be lower [8,14,17]. This is supported by the finding that the ZnO NPs prepared in ethanol (Fig.3) had a considerable fraction of metallic zinc phase, which can be explained by much lower oxidizing abilities of ethanol compared to those of water and agrees with our previous report [17]. Such NPs, with metallic Zn inclusions, are believed to be less prone to aggregation and re-crystallization compared to their counterparts based on single-phase ZnO. This also explains why the NPs prepared in ethanol were spherical rather than rod-shaped: having metallic inclusions, they could not recrystallize as pure ZnO rods. On the other hand, one should keep in mind that ethanol molecules might have acted as surface modifier and passivate forming NPs, thus somewhat suppressing their aggregation.

To lend support to the above assumptions, we carried out a series of additional experiments in which either starch was added into water or some water was added to ethanol. Starch was previously shown to passivate ZnO NPs during their generation via LAL [35], and thus its addition was expected to suppress nanorod formation. As well seen in Supplementary Information Fig.S2c, indeed, no ZnO nanorods were observed after the experiment. In the other experiment, an ethanol-water (9:1 v/v) mixture was used as a medium instead of pure ethanol. As shown in Supplementary Information Figs.S3b,c, this

led to the formation of ZnO nanorods in the product. This proves that the presence of water is essential for the formation of ZnO nanorods, as even as much as 10% of water in the liquid medium was enough to oxidize Zn species and lead to ZnO NPs recrystallized into nanorods.

When ethanol was used as medium, the diameter of generated NPs is seen in Fig.3d to increase with pulse width. Similar to the case with the length of ZnO nanorods in Fig.2, this finding can also be attributed to the effect of somewhat elevated medium temperatures. Although the agglomeration of NPs forming during ablation of Zn in ethanol was believed to be somewhat suppressed, it still contributed into NP growth and was more efficient at higher temperatures (associated with longer laser pulses and more intense energy absorption by the Zn target). Indeed, our measurements confirmed that when the pulse duration was changed from 0.5 to 2.0 ms, the temperature of ethanol after 30-min-long experiments increased from 66 to 77 ^{o}C, almost reaching the boiling point of ethanol.

Figure 4 shows XRD patterns of samples prepared under different conditions both in water (a) and ethanol (b) media. Here, as well as in Figs.5,6 and 7a, red, black and blue colors are used to indicate samples prepared at pulse duration of 0.5, 1 and 2 ms, respectively. In a similar way, solid and dashed lines denote samples fabricated at pulse peak power of 1 and 5 kW, respectively. In Fig.4, the peak positions of hexagonal wurtzite ZnO and Zn phases are marked with vertical pink and green lines, respectively [37], while those of Si substrate are marked with dashed black lines. Based on the XRD patterns in Fig.4 and in agreement with previously published results on LAL-generated ZnO NPs [7,9,10,17,18,35,36], ZnO nanostructures were prepared in water (Fig.4a,b), while those prepared in ethanol demonstrated a Zn phase (Fig.4c). It should be noted that XRD patterns of some samples prepared in water occasionally showed the presence of metallic zinc phase too (see, e.g., Fig.4a, pattern 2 from top). Although a better understanding of this finding may need additional investigations, it is believed to be

explained by the nature of the processes occurring when millisecond lasers are exploited. As was previously demonstrated by Niu *at al*. [8,14], nano-sized droplets of molten metal are typically produced by millisecond-long pulses, which then are fragmented and released loose into the liquid where they are oxidized by the reactive medium such as water. Thereofore, we assume that at higher pulse peak power of 5 kW, some of such metallic zinc droplets were not fragmented well to be oxidized completely. This may also explain why no metallic zinc phase was observed when lower pulse peak energy of 1 kW was used.

Figure 5 demonstrates absorption spectra of colloidal suspensions prepared in water (a) and ethanol (b). Peaks derived from ZnO and metallic Zn are marked with vertical pink and green lines, being at 380 and 280 nm, respectively. The spectra presented in Fig.5 agree well with the results of XRD measurements discussed above, as they also confirm that the ZnO phase dominates in the structures prepared in water, while metallic Zn inclusions emerge in those prepared in ethanol. It is worth noting that some of products prepared in water also demonstrated small amounts of metallic Zn, as seen in Fig.5a. Since the peak at 280 nm results from plasmonic property of metallic Zn [41], it is probably indicative of metallic inclusions inside such nanostructures. On the other hand, the broad shoulder observed at 380 nm in Fig.5b implies that the products prepared in ethanol also included ZnO, which is well consistent with the XRD patterns in Fig.4b. Thus, both X-ray diffraction and absorption spectroscopy analyses demonstrated that, similar to our previous findings for samples prepared by nanosecond pulsed laser [17], the reactivity of liquid medium is also a critical factor determining the phase composition of nanostructures prepared by means of millisecond-long pulses.

Figure 6 presents XPS spectra of the samples, as they were drop-cast on a Si wafer and naturally dried in air. Spectra of samples prepared in water and ethanol are displayed in panels (a,b) and (c,d),

respectively. The spectra are shown for samples prepared at different laser parameters, while positions of corresponding peaks are indicated with the same colors and in the same manner as the data previously presented in Figs.4,5. The vertical lines in Figs. 6a,c and Figs.6b,d, where narrow scans for O 1s and Zn 2p3 peaks are given, indicate the positions of Zn-O (pink), O-C (violet), O-H (orange), Zn-Zn (light blue) and $Zn(OH)_2$ (green) bonding. The chemical bonding states in the nanostructures prepared under different conditions are seen to be tuned via changing laser parameters (pulse peak power and pulse width) and liquid medium used. All the samples prepared via ablating Zn targets with millisecond pulsed laser are seen in Fig.6 to have a significant amount of OH groups on their surface. Interestingly, the fraction of hydroxylated Zn is higher in nanostructures prepared at lower pulse peak power (1 kW) in water and in those prepared at higher pulse peak power (5 kW) in ethanol. This might be explained by the fact that $Zn(OH)_2$ is always the first stage during the ZnO formation via laser ablation of Zn in liquids, with further dehydration to form ZnO being a reversible process [7,10,42,43]. Therefore, it can be assumed that more zinc hydroxide species should be expected in less oxidative media (ethanol). In water, complex changes in oxidative states were observed when laser parameters were varied. The surface of the products prepared at 1 kW are seen in Fig.6a to be oxidized and hydroxylated, tending to be less hydroxylated and shifting to oxide state when laser pulses with 5 kW were used. The use of pulses with higher energy stimulates dehydration of $Zn(OH)_2$ forming in the product and its transformation into ZnO phase.

Figure 7a exhibits PL spectra of the samples prepared in water, while fractions of various defects present in the samples as a function of pulse width at peak pulse powers of 1 kW and 5 kW are shown in Fig.7b and Fig.7c, respectively. The latter defects were evaluated through deconvolution of the PL spectra, as shown in Fig.7a and in agreement with previously published reports [17,27,38]. All the spectra presented in Fig.7a were normalized, while colors and solid or dashed lines are prescribed to PL spectra

of the samples in the same manner as those in Figs.4-6. The dotted color curves underneath the red spectrum represent the results of its curve-fitting (bottom of Fig.7a). In accordance with the previous report of Goto *at al*. [17], seven Gaussian curves were used to fit the spectra, each of which corresponding to various defects in ZnO nanostructures [17,27,38]. The peak in the UV range is derived from the band-edge emission (depicted as "exciton" emission for simplicity) [38,44]. The peak at 450-500 nm shows Zn-related defects, corresponding to transition between conduction band and Zn vacancies (V_{Zn}), interstitial Zn (Zn_i) to valence band, Zn_i and V_{Zn} [17,38]. The peaks around 505, 550, and 630 nm are the features of singly-charged oxygen vacancies (V_O^+), doubly-charged oxygen vacancies (V_O^{++}) and surface defects, respectively [17, 27]. As clearly seen in Fig.7, PL emission related to surface defects (black circles in Figs.7b,c) and doubly-charged oxygen vacancies (V_O^{++}, red circles in Figs.7b,c) dominate in the ZnO nanorods prepared in water. At the same time, the sample prepared at 1 kW and 0.5 ms is seen in Fig.7a to demonstrate a stronger emission caused by Zn-related defects, which is probably explained by a lower laser fluence and lower medium temperature during its preparation. Although the surface-related and V_O^{++} -related defects (black and red circles in Fig.7b) are still dominant in this sample, similar to the others presented in Fig.7a, other defects such as V_{Zn} and Zn_i are also formed and manifest themselves at relatively higher level (Fig.7b, blue and green circles).

Figures 7b,c demonstrate how the fraction of each defect emitting in the PL spectra in Fig.7a changes as a function of pulse width at peak pulse power of 1 kW (b) and 5 kW (c). The fractions of integrated areas for each peak (whose position is indicated by vertical lines in Fig.7a) are shown with the same color that is used in panel (a) for the corresponding Gaussian peak. At 1 kW, as pulse width increases, the density of the majority of emitting defects decreases or remains mainly unchanged, while that for the V_O^{++} related defects increases (red circles in Fig.7b). The main changes in defect density redistribution

observed in Fig.7b for the samples prepared at 0.5 ms and longer should be explained by higher temperatures of water medium caused by longer pulses.

The intensity of the exciton emission (purple circles) is seen in Fig.7c to increase monotonously with pulse duration at larger peak power (5 kW) applied. This enhancement of the exciton-related emission is probably caused by metallic inclusions into ZnO nanorods, in agreement with the previous report of others [39]. Traces of such metallic zinc inclusions into the ZnO samples were observed by XRD and absorption measurements and revealed in Fig.4a and Fig.5. At the same time, the exciton emission is expected to be also affected by the V_O^{++} defects (red circles). However, the latter defects should be gradually eliminated as NPs gradually recrystallize into ZnO nanorods at elevated temperatures, which is not observed in Figs.7b,c.

The fraction of surface defects (black circles in Figs.7b,c) remains mainly unchanged and independent on pulse width and pulse peak power, which is probably related to the shapes of the nanorods that did not change dramatically. There is also no significant redistribution in defect fractions observed for samples prepared with pulses as long as 1 and 2 ms, which is probably explained by the observation that water medium was hotter at such pulse widths used, reaching 70-90 ^oC, while it was always slightly cooler when shorter pulses were applied. Thus, as discussed above, the main factors influencing the difference in defect distribution between samples prepared with shorter (0.5 ms) and longer pulses (1 and 2 ms) are higher medium temperatures and higher influence of fragmentation. The formation energy of V_o^{++} is known to be lower compared to that of Zn_i defects [45]. This may explain why at 1 kW, as the medium temperature rises along with pulse width from 0.5 to 1 and 2 ms, V_o^{++} defects appear to become more favorable while the number of Zn_i defects decreases (red and yellow circles in Fig.7b). At the same time, as the ZnO nanorods are exposed to secondary irradiation with higher-energy pulses (at 5 kW), they

are believed to be fragmented due to photoexcitation accompanied with more intense heating. This might cause partial heat-induced dissociation to Zn and O atoms and further segregation of Zn atoms from ZnO [46], which in turn might result in the appearance of Zn-related defects, as well as inclusions of metallic phase in nanorods.

4. Conclusions

In conclusion, the use of millisecond-long pulses to ablate zinc in water or ethanol was found to provide nanostructures with various shapes, sizes, phase composition and defects. While the use of laser beams with shorter pulses (nanosecond or femtosecond range) previously reported by others typically led to ZnO nanoparticles prepared in water, ZnO nanorods were produced in this study. The growth of such rod-like nanostructures is explained by a temperature raise of the liquid environment caused by long-pulse irradiation of the target. By changing pulse width (0.5 - 2 ms) and peak pulse power (1 - 5 kW), ZnO nanorods with aspect ratios from 1.6 to 6 were prepared. In parallel, spherically shaped nanoparticles were produced in ethanol medium, with metallic Zn inclusions well detected by X-ray diffraction and diameters controlled via laser pulse width. XPS measurements confirmed that the surface chemistry of the products was dependent on laser parameters used. The latter laser parameters were also found to influence the density of various defects in the generated ZnO nanorods, which resulted in control over photoluminescent emission from such nanostructures. The demonstrated control over the shape, size, phase composition and photoluminescent properties of the produced ZnO nanostructures is believed to be attractive for numerous applications.

Acknowledgements. The authors are grateful to the Japan Society for the Promotion of Science (JSPS) for support of this research (grant numbers 16K04904, 15K17431 and 24560882). S.A.K. acknowledges support from

the Seventh Framework Programme (FP7-PEOPLE-2012-IIF, project no. 330516). Finally, S.A.K. and A.G.R. are grateful to the Daiwa Anglo-Japanese Foundation (Daiwa Foundation Award 11425/12174).

References:

[1] Z. Yan and D.B. Chrisey, Pulsed laser ablation in liquid for micro-/nanostructure generation. *J. Photochem. Photobiol. C,* 2012, **13**, 204-223.

[2] H.B. Zeng, X.W. Du, S.C. Singh, S.A. Kulinich, S.K. Yang, J.P. He and W.P. Cai, Nanomaterials via laser ablation / irradiation in liquid: A review. *Adv. Funct. Mater*., 2012, **22**, 1333-1353.

[3] W.J. Qin, J. Sun, J. Yang and X.W. Du, Control of Cu-doping and optical properties of ZnO quantum dots by laser ablation of composite targets. *Mater. Chem. Phys*., 2011, **130**, 425-430.

[4] D. Dorranian, E. Solati and L. Dejam, Photoluminescence of ZnO nanoparticles generated by laser ablation in deionized water. *Appl. Phys. A*, 2012, **109**, 307-314.

[5] K.K. Kim, D. Kim, S.K. Kim, S.M. Park and J.K. Song, Formation of ZnO nanoparticles by laser ablation in neat water. *Chem. Phys. Lett*., 2011, **511**, 116-120.

[6] H.S. Desarkar, P. Kumbhakar and A.K. Mitra, One-step synthesis of Zn/ZnO hollow nanoparticles by the laser ablation in liquid technique. *Laser Phys. Lett*., 2013, **10**, 055903.

[7] Y. Ishikawa, Y. Shimizu, T. Sasaki and N. Koshizaki, Preparation of zinc oxide nanorods using pulsed laser ablation in water media at high temperature. *J. Colloid Interface Sci*., 2006, **300**, 612-615.

[8] K.Y. Niu, J. Yang, S.A. Kulinich, J. Sun, H. Li and X.W. Du, Morphology control of nanostructures via surface reaction of metal nanodroplets. *J. Am. Chem. Soc*., 2010, **132**, 9814-9819.

[9] K. Kawabata, Y. Nanai, S. Kimura and T. Okuno, Fabrication of ZnO nanoparticles by laser ablation of sintered ZnO in aqueous solution. *Appl. Phys. A*, 2012, **107**, 213-220.

[10] B.C. Lin, P. Shen and S.Y. Chen, ZnO and ε–$Zn(OH)_2$ composite nanoparticles by pulsed laser ablation on Zn in water. *J. Phys. Chem. C*, 2011, **115**, 5003-5010.

[11] W.J. Qin, S.A. Kulinich, X.B. Yang, J. Sun and X.W. Du, Preparation of semiconductor nanospheres by laser-induced phase separation. *J. Appl. Phys*., 2009, **106**, 114318.

[12] A.I. Savchuk, A. Perrone, A. Lorusso, I.D. Stolyarchuk, O.A. Savchuk and O.A. Shporta, ZnMnO diluted magnetic semiconductor nanoparticles: Synthesis by laser ablation in liquids, optical and magneto-optical properties. *Appl. Surf. Sci*., 2014, **302**, 205-208.

[13] M.H. Mahdieh and B. Fattahi, Size properties of colloidal nanoparticles produced by nanosecond pulsed laser

ablation and studying the effects of liquid medium and laser fluence. *Appl. Surf. Sci*., 2015, **329**, 47-57.

[14] K.Y. Niu, J. Yang, S.A. Kulinich, J. Sun and X.W. Du, Hollow nanoparticles of metal oxides and sulfides: Fast preparation via laser ablation in liquid. *Langmuir*, 2010, **26**, 16652-16657.

[15] N. Tarasenka, A. Butsen, V. Pankov and N. Tarasenko, Structural defects and magnetic properties of gadolinium silicide nanoparticles synthesized by laser ablation technique in liquid. *Phys. Status Solidi B*, 2013, **250**, 809-814.

[16] S.V. Rao, G.K. Podagatlapalli and S. Hamad, Ultrafast laser ablation in liquids for nanomaterials and applications. *J. Nanosci. Nanotechnol.,* 2014, **14**, 1364-1388.

[17] T. Goto, M. Honda, S.A. Kulinich, Y. Shimizu and T. Ito, Defects in ZnO nanoparticles laser-ablated in water-ethanol mixtures at different pressures. *Jpn. J. Appl. Phys.,* 2015, **54**, 070305.

[18] S.A. Kulinich, T. Kondo, Y. Shimizu and T. Ito, Pressure effect on ZnO nanoparticles prepared via laser ablation in water. *J. Appl. Phys*., 2013, **113**, 033509.

[19] K. Urabe, T. Kato, S. Stauss, S. Himeno, S. Kato, H. Muneoka, M. Baba, T. Suemoto and K. Terashima, Dynamics of pulsed laser ablation in high-density carbon dioxide including supercritical fluid state. *J. Appl. Phys*., 2013, **114**, 143303.

[20] M. Koizumi, S.A. Kulinich, Y. Shimizu and T. Ito, Slow dynamics of ablated zone observed around the density fluctuation ridge of fluid medium. *J. Appl. Phys*., 2013, **114**, 214301.

[21] J.W. Fang, H.Q. Fan, Y. Ma, Z. Wang and Q. Chang, Surface defects control for ZnO nanorods synthesized by quenching and their anti-recombination in photocatalysis. *Appl. Surf. Sci.*, 2015, **332**, 47-54.

[22] Y.S. Fu, X.W. Du, S.A. Kulinich, J.S. Qiu, W.J. Qin, R. Li, J. Sun and J. Liu, Stable aqueous dispersion of ZnO quantum dots with strong blue emission via simple solution route. *J. Am. Chem. Soc*., 2007, **129**, 16029- 16033.

[23] A.B. Djurišić, Y.H. Leung, K.H. Tam, Y.F. Hsu, L. Ding, W.K. Ge, Y.C. Zhong, K.S. Wong, W.K. Chan, H.L. Tam, K.W. Cheah, W.M. Kwok and D.L. Phillips, Defect emission in ZnO nanostructures. *Nanotechnology*, 2007, **18**, 095702.

[24] Y.S. Fu, Y.F. Song, S.A. Kulinich, J. Sun, J. Liu and X.W. Du, Single-crystal ZnO flocky sphere formed by three-dimensional oriented attachment of nanoparticles. *J. Phys. Chem. Solids*, 2008, **69**, 880-883.

[25] S. Kundu, S. Sain, M. Yoshio, T. Kar, N. Gunawardhana and S.K. Pradhan, Structural interpretation of chemically synthesized ZnO nanorod and its application in lithium ion battery. *Appl. Surf. Sci*., 2015, **329**, 206-211.

[26] J.Z. Song, S.A. Kulinich, J. Yan, Z.G. Li, J.P. He, C.X. Kan and H.B. Zeng, Epitaxial ZnO nanowire-on-nanoplate structures as efficient and transferable field emitters. *Adv. Mater*., 2013, **25**, 5750-5755.

[27] X.Y. Xu, C.X. Xu, Y. Lin, J. Li and J.G. Hu, Comparison on photoluminescence and magnetism between two kinds of undoped ZnO nanorods. *J. Phys. Chem. C*, 2013, **117**, 24549-24553.

[28] Z.L. Wang, Zinc oxide nanostructures: growth, properties and applications. *J. Phys.: Cond. Matter.,* 2004, **16**, R829-R858.

[29] C. Langhammer, M. Schwind, B. Kasemo and I. Zorić, Localized surface plasmon resonances in aluminum nanodisks. *Nano Lett*., 2008, **8**, 1461–1471.

[30] J.Z. Song, S.A. Kulinich, J.H. Li, Y.L. Liu and H.B. Zeng, A general one-pot strategy for the synthesis of high-performance transparent-conducting-oxide nanocrystal inks for all-solution-processed devices. *Angew. Chem. Int. Ed*., 2015, **54**, 462-466.

[31] A. Pimentel, D. Nunes, P. Duarte, J. Rodrigues, F.M. Costa, T. Monteiro, R. Martins and E. Fortunato, Synthesis of long ZnO nanorods under microwave irradiation or conventional heating. *J. Phys. Chem. C*, 2014, **118**, 14629-14639.

[32] G. Xu, X.L. Wang and G.Z. Liu, Facile solvothermal synthesis of abnormal growth of one-dimensional ZnO nanostructures by ring-opening reaction of polyvinylpyrrolidone. *Appl. Surf. Sci*., 2015, **329**, 137-142.

[33] M. Distaso, M. Mačković, E. Spiecker and W. Peukert, Formation and dissolution of twin ZnO nanostructures promoted by water and control over their emitting properties. *Chem. – Eur. J*., 2014, **20**, 8199-8209.

[34] E. Chelnokov, M. Rivoal, Y. Colignon, D. Gachet, L. Bekere and F. Thibaudau, Band gap tuning of ZnO nanoparticles via Mg doping by femtosecond laser ablation in liquid environment. *Appl. Surf. Sci*., 2012, **258**, 9408-9411.

[35] R. Zamiri, A. Zkaria, H. Abbastabar Ahangar, M. Darroudi, A. Khorsand Zak and G.P.C. Drummen, Aqueous starch as a stabilizer in zinc oxide nanoparticle synthesis via laser ablation. *J. Alloy. Compd*., 2012, **516**, 41-48.

[36] P. Wagener, S. Faramarzi, A. Schwenke, R. Rosenfeld and S. Barcikowski, Photoluminescent zinc oxide polymer nanocomposites fabricated using picosecond laser ablation in an organic solvent. *Appl. Surf. Sci*., 2011, **257**, 7231-7237.

[37] J. Q. Hu, Q. Li, X. M. Meng, C. S. Lee and S.T. Lee, Thermal reduction route to the fabrication of coaxial Zn/ZnO nanocables and ZnO nanotubes, *Chem. Mater*., 2003, **15**, 305-308.

[38] S. Vempati, J. Mitra and P. Dawson, One-step synthesis of ZnO nanosheets: a blue-white fluorophore, *Nanoscale*

Res. Lett., 2012, **7**, 470.

[39] M.K. Lee and H.F. Tu, Ultraviolet emission blueshift of ZnO related to Zn, *J. Appl. Phys*., 2007, **101**, 126103.

[40] H.W. Jeong, S.Y. Choi, S.H. Hong, S.K. Lim, D.S. Han, A. Abdel-Wahab and H.W. Park, Shape-dependent charge transfers in crystalline ZnO photocatalysts: rods versus plates. *J. Phys. Chem. C*, 2014, **118**, 21331-21338.

[41] H. Amekura, N. Umeda, K. Kono, Y. Takeda, N. Kishimoto, C. Buchal and S. Mantl, Dual surface plasmon resonances in Zn nanoparticles in SiO_2: an experimental study based on optical absorption and thermal stability, *Nanotechnology*, 2007, **18**, 395707.

[42] H.B. Zeng, W.P. Cai, J.L. Hu, G.T. Duan, P.S. Liu and Y. Li, Violet photoluminescence from shell layer of Zn/ZnO core-shell nanoparticles induced by laser ablation. *Appl. Phys. Lett*., 2006, **88**, 171910.

[43] A.L. Zhu, D. Duch, G.A. Roberts, S.X.X. Li, H.J. Wang, K. Duch, E.J. Bae, K.S. Jung, D. Wilkinson and S.A. Kulinich, Increasing the electrolyte capacity of alkaline Zn-air fuel cells via scavenging zincate with $Ca(OH)_2$. *ChemElectroChem*, 2015, **2**, 134-142.

[44] K.-S. Kao, W.-C. Shih, W.-T. Ye and D.-L. Cheng, Photoluminescence of ZnO thin films deposited at various substrate temperatures. *Thin Solid Films*, 2016, **605**, 77-83.

[45] F. Oba, M. Choi, A. Togo and I. Tanaka, Point defects in ZnO: an approach from first principles. *Sci. Technol. Adv. Mater*., 2011, **12**, 034302.

[46] R. Palumbo, L. Lede, O. Boutin, E. E. Ricart, A. Steinfeld, S. Moller, A. Weidenkaff, E.A. Fletcher and J. Bielicki, The production of Zn from ZnO in a high- temperature solar decomposition quench process – I. The scientific framework for the process. *Chem. Eng. Sci*., 1998, **53**, 2503-2517.

Figure captions:

Figure 1. Experimental setup used in this study with millisecond pulsed Nd:YAG laser ablating the surface of Zn plate immersed in liquid media (water and ethanol).

Figure 2. TEM images of nanostructures prepared in water at different pulse width and peak power values. Samples shown in (a-c) and (d-f) were generated at pulse peak power of 1 and 5 kW, respectively. Panels (a, d), (b, e), and (c, f) correspond to samples prepared at pulse width values of 0.5, 1 and 2 ms, respectively. Scale bars indicate 100 nm. Panels (g,h) demonstrate the effect of pulse width on longitudinal (open circles) and short (open triangles) axes (g) and aspect ratio (h) of the ZnO nanorods shown in (a-f). Red and blue markers indicate peak power of 1 and 5 kW, respectively.

Figure 3. TEM images of nanostructures prepared in ethanol at different pulse width: (a) 0.5, (b) 1, and (c) 2 ms. Applied peak power was 5 kW. Scale bars indicate 100 nm. Influence of pulse width on average diameter of produced particles is presented in panel (d).

Figure 4. XRD patterns of nanostructures prepared in water (a) and ethanol (b). Red, black, and blue lines correspond to samples prepared at pulse widths of 0.5, 1, and 2 ms, respectively. Solid and dashed lines correspond to samples prepared at 1 and 5 kW, respectively. A gray XRD pattern in (a) corresponds to Si substrate. Vertical solid pink and green lines correspond to peaks of hexagonal ZnO and metallic Zn, respectively, while dotted black line indicates the position of Si peaks.

Figure 5. Absorption spectra of samples prepared in water (a) and ethanol (b). Red, black and blue lines denote the pulse widths of 0.5 , 1, and 2 ms, respectively. Solid and dashed lines indicate samples prepared at laser powers of 1 kW and 5 kW, respectively.

Figure 6. XPS spectra of the products prepared in water (a, b) and ethanol (c, d). Spectra of samples prepared at peak power of 1 and 5 kW presented with solid and dashed lines, respectively, while those of samples prepared at pulse duration of 0.5, 1 and 2 ms are shown with red, black and blue color, respectively. Narrow scans for O 1s (a, c) and Zn 2p3 (b, d) peaks are presented. Vertical lines stand for ZnO (pink), OC (violet), OH (orange), metallic Zn (light blue) and $Zn(OH)_2$ (pink) species.

Figure 7. Photoluminescence spectra (a) and fractions of each emitting component (b, c) for ZnO nanostructures prepared in water at different laser parameters. In panel (a), red, black, and blue colors denote samples prepared at 0.5, 1, and 2 ms, respectively, while solid and dashed lines indicate those prepared at 1 and 5 kW, respectively. Dotted spectra are the Gaussian curves obtained through the deconvolution of the red spectrum, corresponding vertical color lines indicating the peak positions and the nature of their sources. Panels (b, c) exhibit the effect of laser pulse width at peak power 1 (b) and 5 kW (c) on the defects detected in the ZnO products. The colors shown in (b) and (c) correspond to

emission attributed to exciton, vacancies of Zn (V_{Zn}) , interstitial Zn (Zn_i), both Zn_i and V_{Zn} defects, vacancies due to singly- and doubly-charged oxygen (V_O^+, V_O^{++}), and surface defects.

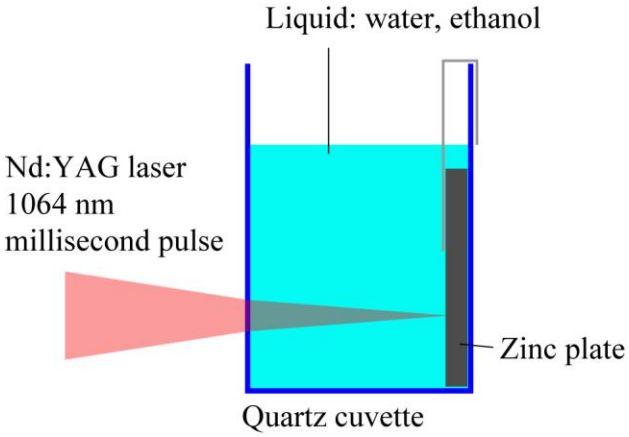

Figure 1. Experimental setup used in this study with millisecond pulsed Nd:YAG laser ablating the surface of Zn plate immersed in liquid media (water and ethanol)

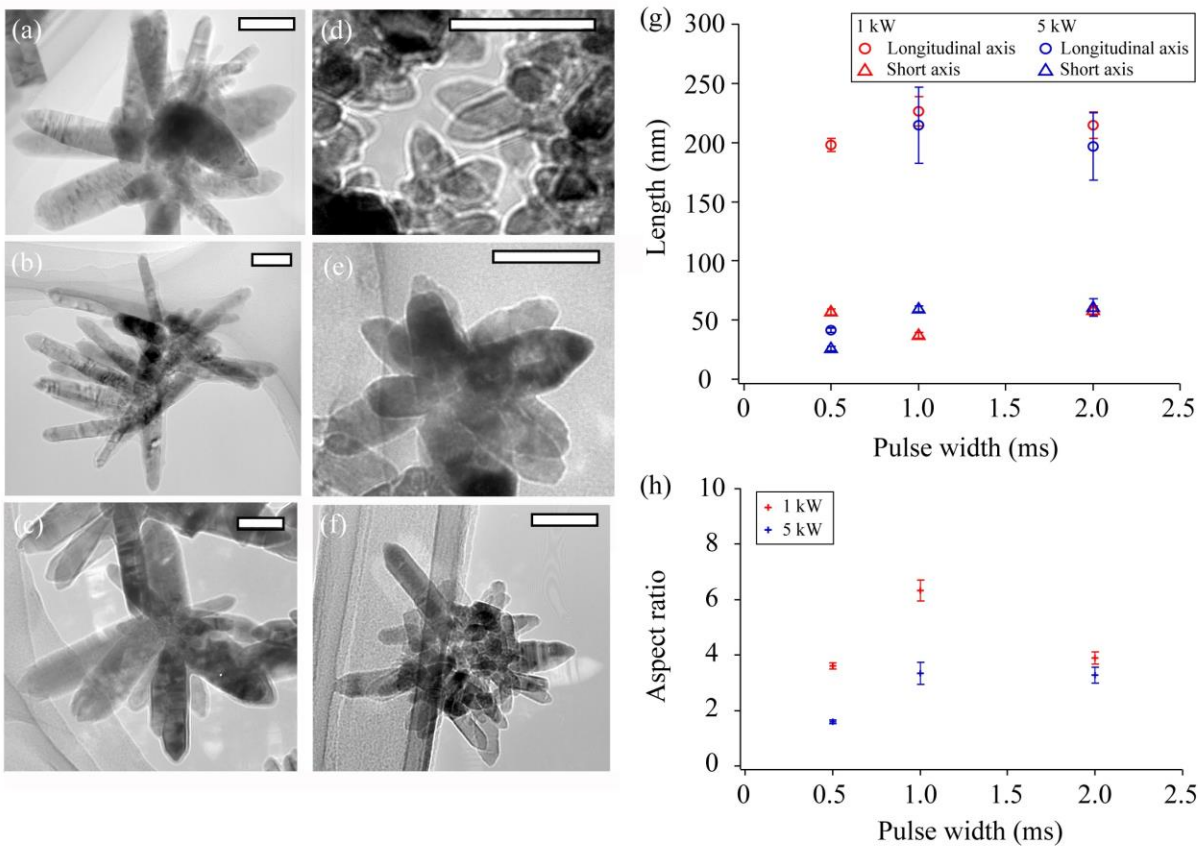

Figure 2. TEM images of nanostructures prepared in water at different pulse width and peak power values. Samples shown in (a-c) and (d-f) were generated at pulse peak power of 1 and 5 kW, respectively. Panels (a, d), (b, e), and (c, f) correspond to samples prepared at pulse width values of 0.5, 1 and 2 ms, respectively. Scale bars indicate 100 nm. Panels (g,h) demonstrate the effect of pulse width on longitudinal (open circles) and short (open triangles) axes (g) and aspect ratio (h) of the ZnO nanorods shown in (a-f). Red and blue markers indicate peak power of 1 and 5 kW, respectively.

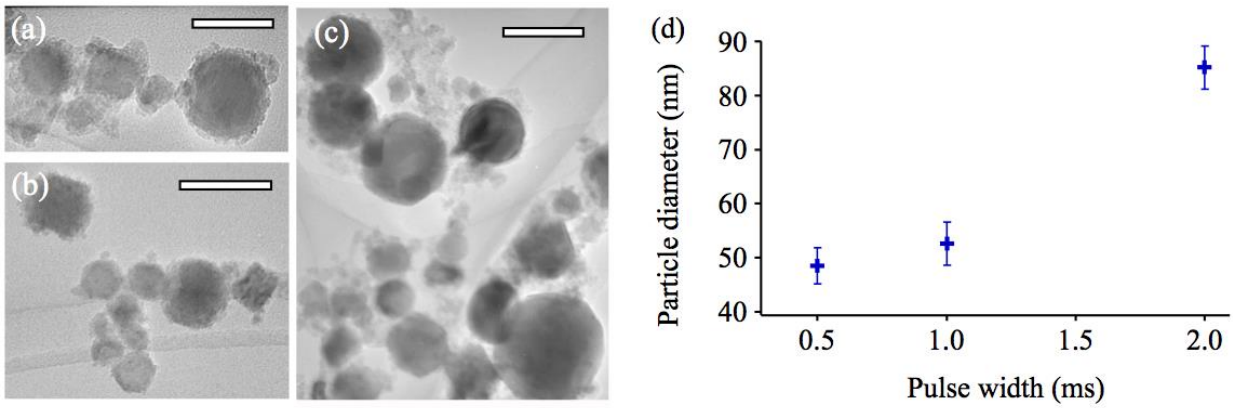

Figure 3. TEM images of nanostructures prepared in ethanol at different pulse width: (a) 0.5, (b) 1, and (c) 2 ms. Applied peak power was 5 kW. Scale bars indicate 100 nm. Influence of pulse width on average diameter of produced particles is presented in panel (d).

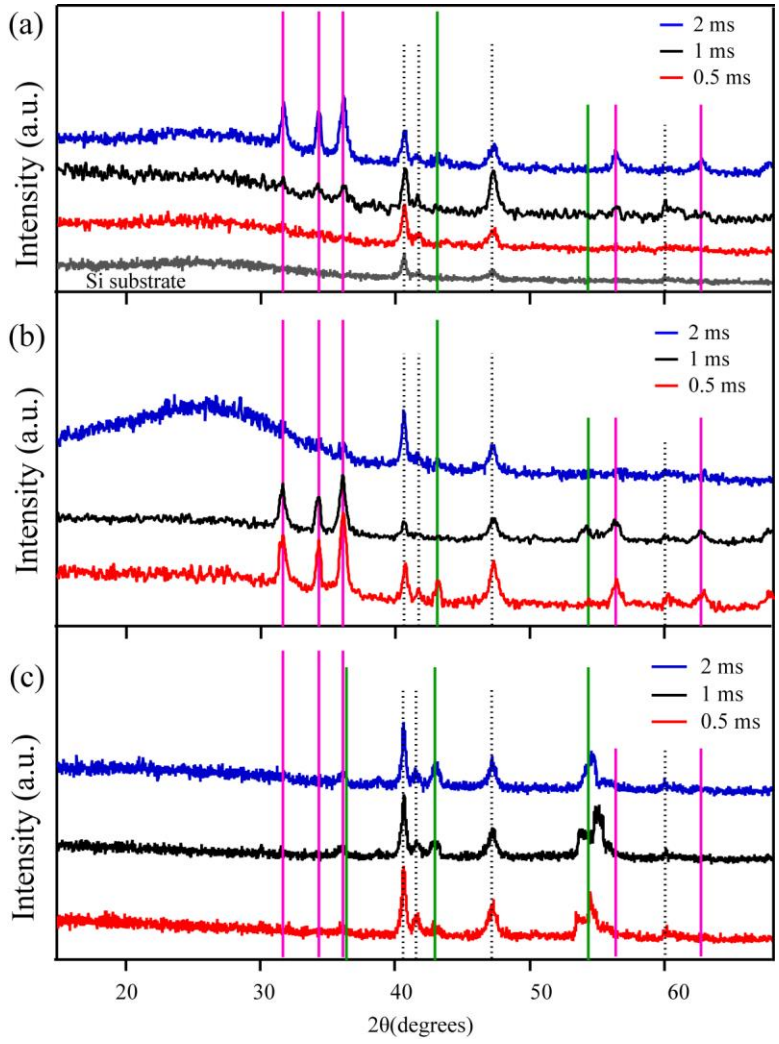

Figure 4. XRD patterns of nanostructures prepared in water (a) and ethanol (b). Red, black, and blue lines correspond to samples prepared at pulse widths of 0.5, 1, and 2 ms, respectively. Solid and dashed lines correspond to samples prepared at 1 and 5 kW, respectively. A gray XRD pattern in (a) corresponds to Si substrate. Vertical solid pink and green lines correspond to peaks of hexagonal ZnO and metallic Zn, respectively, while dotted black line indicates the position of Si peaks.

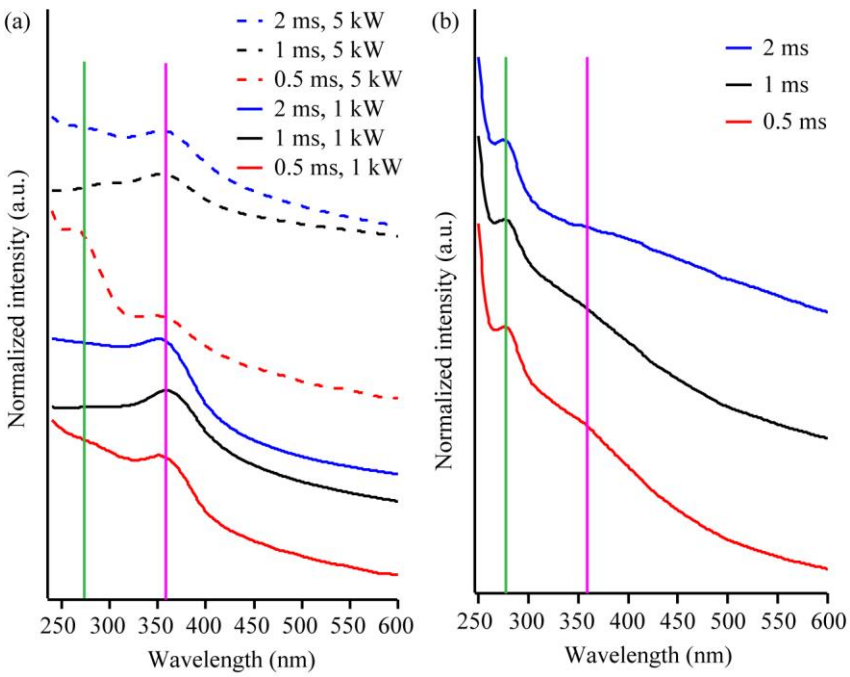

Figure 5. Absorption spectra of samples prepared in water (a) and ethanol (b). Red, black and blue lines denote the pulse widths of 0.5 , 1, and 2 ms, respectively. Solid and dashed lines indicate samples prepared at laser powers of 1 kW and 5 kW, respectively.

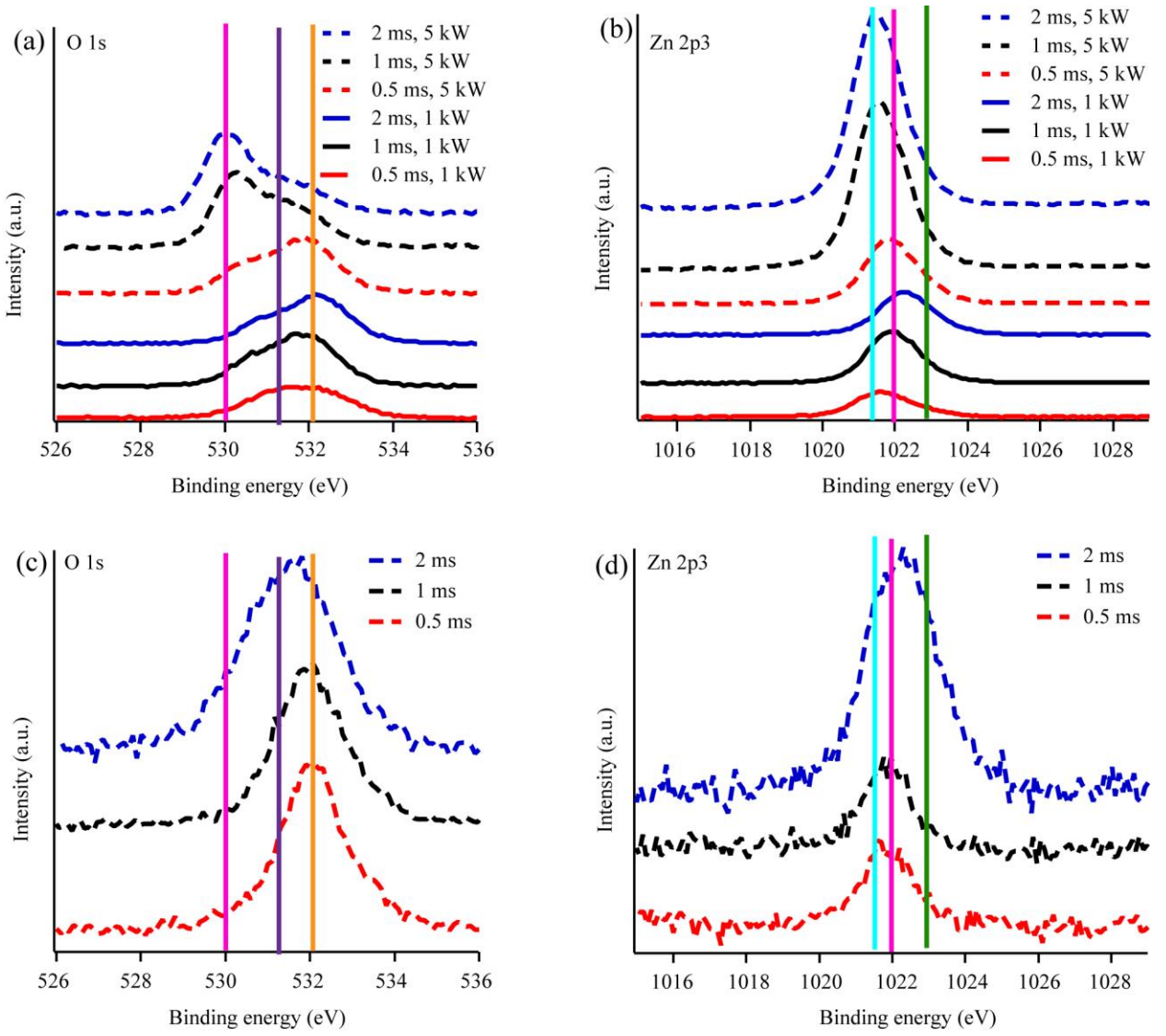

Figure 6. XPS spectra of the products prepared in water (a, b) and ethanol (c, d). Spectra of samples prepared at peak power of 1 and 5 kW presented with solid and dashed lines, respectively, while those of samples prepared at pulse duration of 0.5, 1 and 2 ms are shown with red, black and blue color, respectively. Narrow scans for O 1s (a, c) and Zn 2p3 (b, d) peaks are presented. Vertical lines stand for ZnO (pink), OC (violet), OH (orange), metallic Zn (light blue) and $Zn(OH)_2$ (pink) species.

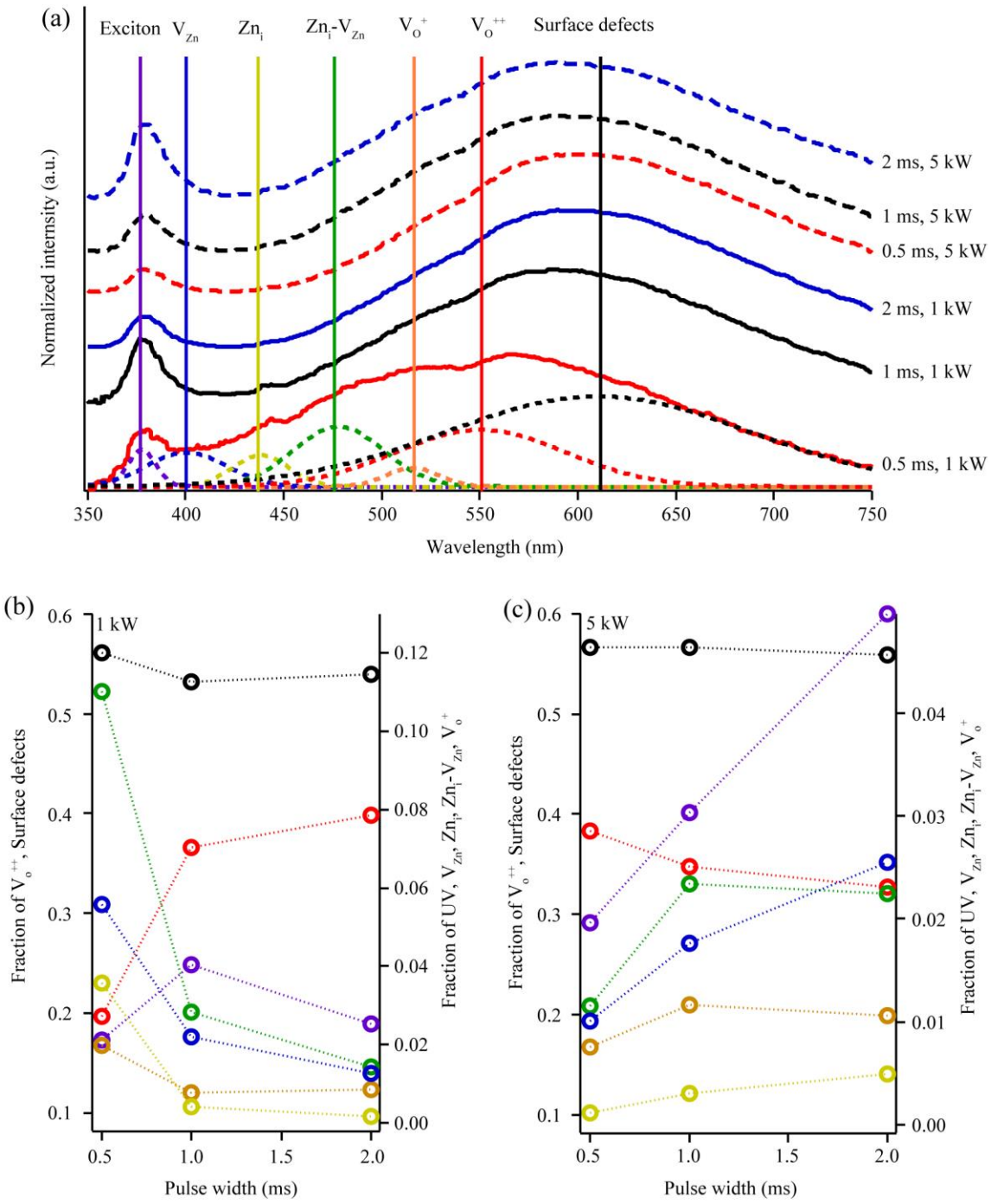

Figure 7. Photoluminescence spectra (a) and fractions of each emitting component (b, c) for ZnO nanostructures prepared in water at different laser parameters. In panel (a), red, black, and blue colors denote samples prepared at 0.5, 1, and 2 ms, respectively, while solid and dashed lines indicate those prepared at 1 and 5 kW, respectively. Dotted spectra are the Gaussian curves obtained through the deconvolution of the red spectrum, corresponding vertical color lines indicating the peak positions and the nature of their sources. Panels (b, c) exhibit the effect of laser pulse width at peak power 1 (b) and 5 kW (c) on the defects detected in the ZnO products. The colors shown in (b) and (c) correspond to emission attributed to exciton, vacancies of Zn (V_{Zn}) , interstitial Zn (Zn_i), both Zn_i and V_{Zn} defects, vacancies due to singly- and doubly-charged oxygen (V_O^+, V_O^{++}), and surface defects.